Revised paper, 13th September 2007

Study on aluminium-based single films

G. S. Vinod Kumar[1,3], F. Garcia-Moreno[1,2], N. Babcsan[1,5], A. H. Brothers[1,2], B. S. Murty[4], J. Banhart[1,2]

1. Hahn-Meitner-Institute Berlin, Glienicker Strasse 100, 14109 Berlin, Germany

2. Technical University Berlin, Hardenbergstrasse 36, 10623 Berlin, Germany

3. Non-Ferrous Materials Technology Development Centre, Hyderabad 500058, India

4. Department of Metallurgical and Materials Eng., Indian Institute of Technology Madras, Chennai 600036, India

5. Bay Zoltan Foundation of Applied Science, BayLOGI Miskolc-Tapolca 3519, Iglói u. 2., Hungary

Abstract

In the present paper the authors studied isolated metallic films made from the same material used for making metallic foams, and then characterised their properties. Metal films were made from a liquid aluminium alloy reinforced with ceramic particles of known concentration. Melts without such particles were also investigated. It is shown that stable films could not be made from Al-Si alloys having no particles and just extremely thin and fragile films could be made from commercially pure Al. In contrast, aluminium alloy containing particles such as SiC and TiB_2 allowed pulling thin, stable films, which did not rupture. Significant thinning of films was observed when the particle concentration in the melt decreased. By in-situ X-ray monitoring of liquid films during pulling, film thickness and drainage effects within the liquid film could be studied. The morphology and microstructure of films was characterised after solidification. Our work shows that the question of how foams are stabilised can be studied using a simplified system such as a film, instead of having to deal with the multitude of different structural elements present in a foam.

Keywords: Metal Foams, Foam films, Composites, Interface, X-ray radioscopy

1. Introduction

Metal foams are a class of materials offering potential for various structural and functional applications [1]. The processing routes of metal foams can be classified into four different categories. They are: liquid state processing, solid state processing, electrochemical deposition, and vapour deposition routes [2]. The liquid processing routes for making closed cell metal foams are popular and widely used, because they are economically attractive and a wide range of metals and alloys can be foamed. However, the phenomena of liquid drainage and melt distribution associated with these processes are major issues during bulk foam production [3]. Thus, it is essential to have a clear scientific understanding of the mechanism of aluminium foam stabilisation in the liquid state, in order to make the production technology more reliable and reproducible.

Aluminium-based metallic foams have been studied both in the liquid and the solid state by means of a large variety of methods. All these methods are essentially integral analyses of a collection of different elements constituting a foam, namely films, Plateau borders and nodes. The properties of the individual elements, such as single films, are at present unknown. The term 'foam stability' is related to the avoidance of cell wall ruptures resulting mainly from perturbations and drainage. From aqueous foams it is known that several factors influence foam stability, including the geometry of Plateau borders, cell wall thickness, surface segregation, surface mobility, dilatational viscosity and elasticity [4]. The decay of a liquid foam starts with cell wall rupture, therefore understanding the phenomena related to the cell wall has the highest importance [5]. To produce stable liquid-metal foam by blowing gas into the melt, a minimum amount of solid particles is necessary [6]. During foaming, process variables such as particle size, particle fraction, and foaming temperature determine the cell size and cell wall thickness [7]. The

particle content in the liquid metal may increase both melt viscosity, which slows down the vertical motion of liquid, and the surface properties of film/gas interfaces as particles segregate there **[8]**. Ip et al. suggest that solid particles lead to flatter curvatures around the Plateau borders, which reduce suction of metal from the cell wall into the border **[6]**. Ceramic particles such as SiC, Al_2O_3, MgO, TiB_2 are mainly used to increase the stability of liquid aluminium foam. Wang and Shi have reported that a critical concentration of SiC or Al_2O_3 is required to achieve foam stability **[7]**. However, no systematic study has been carried out to understand the physics of foam stability in the field of metal foams.

Numerous studies on the phenomenon of foam stability in aqueous foams are available in the literature. Many of these are theoretical works **[9][10]** or numerical process simulations **[11][12]**. Recently, Carrier et al. have experimentally investigated the steady state drainage of liquid in bamboo foam **[13]**. This was to understand the drainage of a liquid soap film, in the absence of the Plateau border. Due to the complexity of foam systems, most attempts to study the fundamental mechanisms of aqueous foaming have been carried out using simple models **[14]**. One of these simple model experiments is vertically pulling a single soap film from a liquid bath using a wire frame. This film has been used to mimic the basic cell wall, and hence studying the drainage and stability of liquid foam using single films is feasible. From the literature available about the model studies of aqueous films, it is clear that the same factors which play a role in foam stability, such as film thickness, elasticity, etc. also appear to have a decisive influence on the stability of isolated soap films **[13]**.

It is thought that films of liquid metal cannot be stretched as thin as aqueous films and that metallic films and liquid-metal cell walls usually rupture below the thickness of 30-150 μm **[8]**. It was found that the cell wall thickness in solidified aluminium foams depends upon the

particle size [7] and the composition of the alloy [8],[15]-[19]. Systematic study is still required to find out the effect of particles on the cell wall thickness of single films.

The present study is taken up in an effort to understand foam stability and related phenomena using single films pulled from the liquid metal. This attempt mainly focuses on metallographic studies of metal film cross sections, in the presence and absence of the stabilizing particles. Drainage in the liquid metal film is also studied in-situ by monitoring single liquid films pulled on wire frames from melts containing Al metal, with and without stabilizing particles.

2. Experimental

2.1 Single metallic films

Single metallic films are made by pulling circular and square wire frames from a liquid metal maintained at constant temperature. For this purpose, commercially-pure aluminium, a commercial AlSi9.5 alloy, a commercial AlSi9.5/SiC particle composite (Al-9.5 wt.% Si-0.6 wt.% Mg containing 20 vol.% SiC of mean size 10 μm, having the trade name F3S20S by Alcan, Montreal, Canada), and Al-6 vol.% TiB_2 composites are chosen for study. The Al/TiB_2 composite is prepared in-house through a flux-assisted synthesis route [20]. In this article we chose the usual designations to specify the composition of a particle-containing alloy, according to which for example 'AlSi9.5/SiC/20p' means: 20 vol.% SiC particles ('p') in the alloy Al-9.5 wt.% Si [21]. For each experiment, 150 g of the precursor was melted in an alumina crucible using an electrical resistance furnace in an open atmosphere. After the melt reached the desired temperature, a stainless steel wire frame, wire thickness 0.2 or 0.4 mm, was inserted into the previously skimmed liquid metal. After holding the wire frame inside the liquid for some time to achieve an equilibrium in temperature, the frame was gently pulled out from the liquid and

allowed to solidify. Solidification took place very fast in the order of a few seconds. The film pulling was done manually, and the pulling velocity was kept very low, to achieve thin and stable films. Films were also made from composites having lesser volume fractions of SiC and TiB_2 particles, made by dilution of the standard composites. For consistency, averages of 10 films were pulled for each experimental condition.

The characteristics of the films were analyzed via metallographic inspection of their cross sections, to study the influence of different stabilizing particle compositions, sizes, and volume fractions on the stability and thickness of the film. The films thus analyzed were sliced vertically through the cross section for metallographic analysis, as shown schematically in Fig. 1. The surfaces of the films were also examined using scanning electron microscopy.

2.2 In-situ X-ray analysis

Drainage in the liquid metal films was studied using in-situ X-ray radioscopy equipment already described in the literature **[22]**. For this purpose, an automatic film pulling apparatus, controlled by a stepper motor and integrated with a resistance heating furnace, has been set up inside the X-ray radioscopy chamber (Fig. 2). The furnace is designed for X-ray observation and consists of two heating elements (carbon layers embedded in silicon nitride) perpendicular to the beam direction, and two boron nitride plates (2 mm thickness) along the X-ray path.

Figure 3 shows the different steps of the in-situ film analysis. The metal wire frame is first immersed into the liquid metal, and then withdrawn slowly, following a considerable equilibration period inside the melt. The liquid film formed in the wire frame is kept approximately isothermally inside the hot zone for acquiring continuous X-ray images. In this case, the films were made using molybdenum and tantalum wire frames (0.5 mm diameter) instead of stainless steel wire, to avoid the reaction between the frame and liquid aluminium,

which took place when holding the films at higher temperature for longer times during image collection.

Quantitative analysis of X-ray images was performed using the software AXIM, described elsewhere **[22]**. This analysis allows us to measure the variation in film thickness with vertical position, for a selected region of interest. Observing in-situ the thickness evolution of a liquid metal film over a longer time, we can get information about possible drainage effects. For this calculation we use the assumption that the intensity I transmitted to our detector follows the Beer-Lambert rule of attenuation:

$$I = I_0 \exp(-\mu d), \tag{1}$$

or

$$\ln(I/I_0) = -\mu d, \tag{2}$$

where μ is the linear absorption coefficient of the metal, I_0 the original X-ray intensity, and d the film thickness. The detector count rate for the unattenuated beam provides a value for I_0. The lowest count rate in the image, I_{min}, we relate to the thickest point of the cell wall, $d_{max.}$ and define the normalised relative film thickness by dividing two expressions (2) by each other:

$$\frac{d}{d_{\max}} = \frac{\ln(I / I_0)}{\ln(I_{\min} / I_0)}. \tag{3}$$

We assumed a linear response of the detector counts to X-ray intensity and a constant value of μ throughout the sample, which therefore cancels. This means that we do not need the absolute value of the linear absorption coefficient μ which contains the coefficients of all the phases present (Al, Al-oxides, SiC) if we are merely interested in relative changes of thickness. A relative comparison of the density before and after a defined time shows us the presence of

drainage, assuming that the detector sensitivity and the thickness of the oxide layer do not change appreciably during the analysis time.

2.3 Texture analysis

Texture analysis was performed in a 4-axis goniometer with an X-ray source from Seiffert (Model Dx-Co100x1-S), having a Co target operating at an accelerating voltage of U = 40 kV and a source current of I = 40 mA, and with a spot size of ~ 2 mm. Pole figures of the Al-films were measured in order to analyze the orientation of the crystalline structure. To scan the whole pole figure, the angles were varied in the range of $0° < \varphi < 360°$ and $0° < \chi < 75°$ with steps of $\Delta\varphi = 10°$ and $\Delta\chi = 5°$.

3. Results

3.1 Microstructural characterisation

Microstructural characterisation for solidified single metal films was conducted to study the particle influence on thickness, surface morphology, and stability of the film, using optical microscopy and scanning electron microscopy. In order to understand the role of particles on the formation of Al metal film, it was decided to make films from pure Al and AlSi9.5 without particles, as well as from AlSi9.5/SiC/20p and Al/TiB_2/6p metal matrix composites.

3.1.1 Films of Al and AlSi9.5 without particles

Figures 4a and 4b show photographs of typical Al films made from commercially-pure Al using both circular and square wire frames. The stainless steel wire frame size is 20 mm in diameter in the circular case, and 20×20 mm^2 in the square case. The pure Al liquid bath was kept at 700 °C and several thin films were pulled at this temperature. The pure Al films obtained after

solidification appeared to be stable and posses uniform thickness throughout the frame area. However, hairline ruptures and transparent regions due to stretching of the film were observed at the film surfaces. Figure 5 shows the surface of one such pure Al film, which reveals transparent regions appearing like stretch marks formed during thinning (lower left panel). At higher magnification (lower right panel), these transparent regions take the appearance of distinct fibres or columns, arranged parallel to the pulling direction. In some places, these fibres are broken due to excessive stretching.

To clarify the crystallographic orientation of the solidified columns on Fig. 5, a (111)-pole figure of the film was measured (Fig. 6). It gives a representative image of the texture in the samples, as the grains, or columns in this case, are much smaller than the X-ray spot on the sample (~ 2 mm). On the pole figure, especially under an angle $\chi \approx 50°$, some (111)-maxima in the pulling direction ($\varphi = 0°$) and perpendicular to it ($\varphi = 90°$) can be found. This reveals an inhomogeneous polycrystalline structure. Furthermore, it suggests that the structure is correlated to the pulling direction. Due to the non-flat, wavy surface of the solidified metallic film there is some expected broadening of the peaks. Also, some peak blurring is caused by the twisting of some columns within the cracked sections, as observed in Fig. 5.

Figure 7a-f show optical micrographs of a pure Al film cross section. The ‘top’ written in these micrographs represents the direction of the top part of the film, i.e., the direction in which the film was pulled. Figure 7a shows the top part of the film cross section, including the node and the Plateau border. The node is the cross section of the wire frame, of 0.2 mm diameter. Figure 7b shows the film formed next to the Plateau border. Subsequent thinning of film is observed from the top towards the centre, represented in Fig. 7c-e. The film thickness measured in this case is ca. 12 μm at the top and ca. 4 μm at the centre of the film. Figure 7f shows an optical

micrograph of the bottommost part of the film. The bottom of the film shows a thicker Plateau border, in comparison to the top. This could be attributed to drainage of liquid metal during film pulling. Figure 7f also shows the part of the film which has cracked due to excessive thinning before and stresses during solidification.

Various temperatures between 650 °C and 700 °C were tried for film pulling from the alloy AlSi9.5 without particles, but in no case a stable film could be made, hence no such film is shown here.

3.1.2 Al alloy films with SiC additions

Figure 8a shows a photograph of AlSi9.5/SiC/20p composite films made using both circular and square wire frames. The stainless steel wire frame size is of 20 mm diameter in the circular case, and 20×20 mm^2 in the square case. The melt in the furnace was maintained at 650 °C during film pulling. This temperature was chosen because no stable film could be made at much higher temperatures (e.g. > 700 °C). The melt was stirred periodically to avoid settling of SiC particles due to gravity. The volume fraction of SiC particles present in the liquid Al-Si alloy was 20 %, and the mean particle size was 10 μm. The surface oxides and slag were removed by proper skimming before introducing the wire frame into the melt. Stable, uniform, thick films could be made without any ruptures.

The surfaces of AlSi9.5/SiC composite films appeared rough, unlike the surface of pure Al films. The SEM micrograph (Fig. 8b) shows wrinkles on the surface of the film. The closer view (Fig. 8c) of the film surface clearly shows small elevations throughout the surface of the film. The metallographic cross section of the film (Fig. 8d) shows that these elevations were due to SiC particle clusters, entrapped in the film during solidification. From the photographs (Fig.

8a), the bottoms of the films appear to be thicker near the frames, in comparison to the tops. This could again be attributed to drainage of liquid, which accumulates at the bottom part of frame and solidifies.

Optical micrographs of the cross section of another AlSi9.5/SiC/20p composite film are shown in Fig. 9a-d. The SiC particles are uniformly distributed throughout the cross section of the film. Figure 9a shows the top part of the film, having a node and Plateau border. The Plateau border contains a large number of SiC particles, evenly distributed in the Al-Si matrix. It is sometimes observed that the SiC particles are arranged in the film such that two or three SiC particles form a column which connect the opposite film surfaces. A 3D analysis in similar foams has shown that such connections are rare in three dimensions **[23]**, but still it seems that the number of particles present in the alloy, and their size, determines the thickness of the film (Fig. 9b and 9c). Based on these observations, it was decided to continue the film pulling experiments by decreasing the volume fraction of SiC particles.

The concentration of SiC particles (20 vol.%) in our composites was decreased to 15, 10 and 5 vol.% by dilution with AlSi9.5. The temperature of melt during film pulling was kept at 650 °C in all cases. The size of the stainless steel wire frames was 20 mm, and the diameter of the wire was 0.2 mm. Stable and thin films, without rupture, were produced from the composite melts containing 20, 15 and 10 % of SiC particles. However, film making was difficult with only 5 vol.% of SiC particles since rupture destroyed the emerging films almost immediately after pulling.

Figure 10 shows optical micrographs of the cross sections of composite films of different volume fraction (20, 15, 10 and 5 vol.%) of SiC particles. The cross-sectional thickness measured in the case of AlSi9.5/SiC composite film (containing 20 vol.% SiC) ranged from 21 μm to

45 μm except for the top and bottom Plateau borders (Fig. 9). This could be attributed to a large number of SiC particles present in the film. Decreasing the SiC particle concentration to 15 % caused a significant decrease in film thickness, to 13–24 μm. It is interesting to note that the film produced from the 10 % SiC composite is the thinnest among all SiC particle concentration studied, with minimum and maximum film thicknesses of 10 μm and 23 μm, respectively. Unlike in the 20 and 15 % SiC composites, only single SiC particles are found between the film surfaces, through the entire cross section of the 10 % composite film. Further decreasing the SiC concentration to 5 % caused problems with film pulling. The cross section shown in Figure 10 is an undamaged partial film obtained by fast withdrawal/pulling of the film, i.e. an artificially preserved instable film. This is to show that very few SiC particles are present between the film surfaces, which do not suffice to stabilize the film.

3.1.3 Al-based films with TiB_2 additions

Al/TiB_2/6p in-situ metal matrix composite prepared in the authors' laboratory was used for making single films. The composite contains submicrometre-size TiB_2 particles, ranging from 0.5 to 2 μm, in a pure Al matrix. Stainless steel wires of 0.2 mm and 0.4 mm diameter were used to make circular and square wire frames. For making films, the molten Al/TiB_2/6p composite was kept at 675 °C. This temperature was chosen because no stable film could be made at higher temperatures. Surface oxides and slag were removed by proper skimming before introducing the wire frame into the melt. Stable, smooth and thin films could be pulled from this melt, without rupture. Figures 11a-d show the metallographic cross section of a film made from Al/TiB_2/6p composite. The TiB_2 particles form networks or clusters, due to their fine size and high concentration in the Al matrix. Figure 11a shows the top part of the film, i.e. the node and Plateau border.

In order to investigate the influence of TiB_2 particle concentration on film thickness, single films were made from Al/TiB_2/3p, Al/TiB_2/1.5p and Al/TiB_2/0.6p composite, again produced by dilution. For pulling films, the liquid metal was kept at 675 °C. Stable films without rupture could be made even from the lowest concentration (0.6 vol.%) of TiB_2 in Al. The surfaces of the Al/TiB_2/0.6p and Al/TiB_2/1.5p films were observed to be smooth, without elevations or surface roughness, in comparison to the surfaces of Al/TiB_2/3p films. Al/TiB_2/0.6p is the thinnest film measured among the three volume fractions studied, as shown by the polished sections in Fig. 12. The minimum film thicknesses measured were 30 μm for 6 %, 37 μm for 3 %, 24 μm for 1.5 %, and 16 μm for the 0.6 % composite. The thickness variation was largest for 6 % TiB_2 and therefore the corresponding value for the minimum thickness is less significant.

The minimum thickness measured in Al/TiB_2/0.6p films is more than that of SiC-stabilized films with 10 vol.% SiC particles, suggesting other factors than just volume fraction. A panoramic view of the metallographic cross sections (Fig. 13) confirms that the thickness of the Al/TiB_2/0.6p film is uniform throughout the cross section, and its lower thickness is highly significant in comparison to the Al/TiB_2/3p film.

3.1.4 Comparison of different films

Table 1 summarises the results of the different film pulling experiments. The interdependence between particle content and film thickness is evident.

3.2 In-situ film thickness and drainage measurements

Radioscopic images of a single film pulled from an AlSi9.5/SiC/5p melt using a square Mo-wire frame are shown in Fig. 14, at a) t = 0 s, and b) after 465 s. The analyzed region of interest (ROI) is marked with a dashed box. The analysis shows that there is a small change over

time (as much as 465 s) in the gravitationally-induced drainage. For this particular sample, we find a sharp increase in film thickness in the lowest 10 mm.

To better illustrate the measured film thickness evolution in time, film thickness changes are shown for selected values of height (i.e., distance from the bottom of the ROI for the square film shown in Fig. 14) in Fig. 15 a-c. In these, the relative thickness of the film (i.e., thickness normalized by the maximum measured thickness) at heights of x = 2, 10, and 18 mm are plotted as functions of time. For x = 2 and 10 mm, small decreases in relative thickness, of ~ 5.1±0.4 % and 8.4±2.0 % respectively, can be observed. For x = 18 mm, an increase in density of 5.3±1.5 % was found.

4. Discussion

4.1 Films of pure aluminium

The aforementioned results clearly show that single films without major damage can be produced from commercially pure Al without any stabilizing particles. This is in contradiction with earlier experiments by Babcsán et al. **[24][26]** who did not obtain stable films when pulling a frame from pure Al melt. The reason could be that in the earlier experiments a much thicker wire (about 1 mm) was used and possibly the temperature was different. It appears that thinner wires make film pulling easier, but this possible effect still has to be explored.

The pure Al films made here are fragile and develop hairline ruptures probably during solidification. As the melt does not contain particles the surface oxide of the Al melt, which forms as a skin over the surface of the film during withdrawal of the frame, must stabilize the pure Al films. Thinning of films could take place due to drainage of liquid Al between the oxide skins on the film surfaces. Due to the absence of particles, liquid drains in excess, causing maximum thinning of film and leading to rupture or cracking before or during solidification. The

metallographic cross sections of the pure Al film (Fig. 7) confirm this although it does not reveal how and when this rupture takes place. In the case that rupture occurs in the liquid state the presence of oxide skins prevents complete rupture of the pure Al film.

This kind of melt surface oxide may be not so strong in case of the Al-Si melt, thus making Al-Si film pulling impossible in the absence of particles. Moreover, the fluidity of the near-eutectic AlSi9.5 melt may be too high and facilitate drainage during pulling.

As a clear directionality in the columnar structure of the solidified films was found (Fig. 5), it is obvious that this structure is related to the pulling direction. Texture analysis showed a clear grain orientation in the film pulling direction. As the samples are taken out from the furnace (in the pulling direction), the solidification front will initiate in the coldest region of the frame, most likely the top of the film, which is first to emerge from the hot zone, and where the rod holding the frame acts as a heat sink. From there, the film seems to solidify directionally towards the bottom. At cracks formed in the oxide skin during solidification, the structure can be observed better, but it is also visible beneath the oxide layer. At defects or trapped particles, it is possible to see that early heterogeneous nucleation takes place, and solidification occurs locally in all directions (Fig. 5 b and d).

4.2 Al alloy films with SiC additions

Single films could be made successfully from AlSi9.5/SiC with different particle volume fractions. Particle accumulation in a foam cell wall plays a key role in the stabilization process. The exact nature of stabilization is hitherto unknown. Two effects are commonly postulated: Firstly, that the particles increase either bulk or surface viscosity, thus retarding drainage in films **[3]**. Secondly, that the particles are partially wetted by the melt and therefore preferentially go to the metal/gas interfaces and give rise to surface forces parallel to the surface **[23]**. Oxide films on

top of the surfaces further increase stability as explained in Fig. 16 of Ref. **[8]**. The two effects are not mutually exclusive and could be both important.

For surface segregation the particles should possess an optimum wetting angle (neither excessive nor poor wettability by molten Al). From non-metallic foams it is known that contact angles ranging from 75°-85° are favourable for foaming but the situation is not clear for metallic foams **[25]**. Moreover, contact angles taken from the literature might not reflect the actual situation of particles in metal foams where additional oxide layers may modify the conditions. Therefore, a discussion of stability based on contact angles is not very promising.

Wrinkles observed in the film surfaces (Fig. 8b) reflect an oxide layer, also found at the cell wall surfaces of Al metal foam when air or oxygen is used as a foaming gas **[25]**. Surface elevations or dimples in the film (Fig. 8c and 8d) are due to SiC particle agglomeration before solidification. Due to these surface dimples, non-uniformity in film thickness has been observed across film cross sections. From the metallographic cross section of the AlSi9.5/SiC film (Fig. 9), it is clear that the SiC volume fraction is a major factor influencing the thickness of the film and its stability.

Thin, stable and smooth films without much surface relief are obtained by decreasing the volume fraction of SiC particles from 20 vol.% to 15 and 10 vol.%. For 5 vol.% SiC particles no entire films could be created, only some small areas by very quick pulling. This could be attributed to a decrease in melt viscosity due to decrease in the particle concentration, which facilitates the liquid flow between the film surfaces, but also to different surface properties of the films which are less densely populated with particles at the metal/gas interface. In addition to the absolute value of thickness, a better uniformity in film thickness is observed when decreasing the volume fraction of the SiC particles.

Thinning of the film below the size of the SiC particles (10 μm) tends to rupture, suggesting the influence of particle size as well. Single particles would bridge the entire film in such cases thus leading to puncture and rupture. In composite films at 5 vol.% SiC, the number of particles found between the film surfaces (Fig. 10) is less, and in some places no particles could be seen. This is the reason why 5 vol.% SiC is not enough to stabilize the film.

Although a reliable measurement of SiC particle distribution within the films is still lacking it seems that surface segregation is less pronounced in the single films compared to foams blown from the same melt. Especially the Plateau borders contain many particles away from the metal/gas interfaces. This can be attributed to the way the structures are created: in foams a bubble rises through the melt and collects particles which immediately adhere to the interface, whereas pulling of the ring does not act in this way. Moreover, the time scale is different: foams usually remain liquid much longer than the films pulled in the current study (minutes compared to seconds) and the particles have more time to rearrange and to segregate.

4.3 Al films with TiB_2 addition

Babcsan et al. in their recent study on submicrometre particle stabilized foam has proved that TiB_2 is a good foam stabilizer, and that it segregates to cell wall surfaces and thereby stabilizes Al foam **[27]**. This also applies to foam produced by a different foaming process based on expanding foamable precursors: TiB_2 particles in Al result in an increase of maximum foam expansion, due to a decrease in the cell wall thickness **[28]**. TiB_2 particles are known to have poor wettability in Al – especially when they have a reacted surface – and so the fact that the TiB_2 particles in the precursors used have been produced in-situ should play an important role. For this reason, it was decided to study single films pulled from Al-6 vol.% TiB_2 in-situ reacted composites. Stable, thin and smooth films can be made from Al-6 vol.% TiB_2 melts. From the

metallographic cross section (Fig. 11) it is clear that TiB_2 particles form clusters, due to their fine size and high concentration. These clusters seem to stabilize the film, instead of single particles. The clusters are found to segregate in the grain boundaries. Decreasing the TiB_2 particle concentration from 6 to 3, 1.5 and 0.6 vol.% in Al decreases TiB_2 cluster size, which tends to the formation of stable and thin film with smooth surfaces. For example, at the lowest concentration of 0.6 vol.% TiB_2, the film thickness was reduced significantly, and was uniform throughout the cross section (Fig. 13). Even 0.6 vol.% of TiB_2 particles in Al could give a thin stable film, with a smooth surface equivalent to pure Al film. It is clear that the thickness of the film decreases significantly with decreasing TiB_2 concentration in Al (Fig. 14). From this observation it is near at hand that the viscosity of the melt plays a major role on thinning of the film (this was further confirmed by the fact that quickly-pulled films were thicker than slowly-pulled ones). At higher concentrations (3 vol.% TiB_2), the viscosity of melt is high, thus the frame catches more liquid, and there is no sufficient time for the liquid to flow out before solidification. This leads to formation of films with non-uniform thickness. In contrast, lower concentrations (0.6 vol.%) of TiB_2 particles in the melt decrease the melt viscosity and increase the liquid flow in between the film surfaces, causing film thinning before solidification. It should be noted that the film thinning is restricted to the particle or cluster size, beyond which the film ruptures.

Comparing films stabilised with SiC and TiB_2 one notes that the minimum volume fraction required for SiC is at least 10 times higher than for TiB_2. The main influence is most likely the alloy. Pure Al can be film pulled even without particles, AlSi9.5 not. Another reason could be the smaller particle size in the Al/TiB_2 composite and the correspondingly much higher number of particles. More and smaller particles more easily cover an interface and are more efficient foam

stabilizers. Therefore the slope $\partial d / \partial c$ (*d:* cell wall thickness, *c:* particle concentration) is larger for TiB_2 than for SiC, i.e. adding TiB_2 is more efficient than adding SiC.

4.4 In-situ film thickness and drainage measurements

Usually, circular films can be pulled from the melt with greater success than square ones. They are more stable and do not rupture as easily during film pulling as square ones. For in-situ analysis, however, square frames were used in order to maximize the fraction of the film falling within the square ROI (Fig. 14). Nevertheless, the first millimetres of the film (nearest to the wire frame) could not be taken into account, as they were too close to the wire frame. The ROI is therefore not a closed system, i.e., the integral of the film thickness is not constant in time, as liquid can flow into or out of the ROI. Drainage is difficult to observe, as in this configuration we could not include the bottommost region, where drained liquid accumulates in a real foam. This seems to be the reason why we see a relative reduction in thickness of 5.1±0.4 to 8.4±2.0 % for x = 2 and 10 mm, respectively; liquid is flowing down the wire and out of the ROI, due to gravity (Fig. 15). And it explains also the 5.3±1.5 % increase of film thickness for x = 18 mm, where liquid stored on the top of the wire is flowing down into the region of interest.

5. Summary and Conclusions

1. Pure aluminium single films could be made, but they were very thin and fragile. The melt surface oxide covers the film and stabilizes it partially, even in the absence of particles. No film could be made from Al-Si alloy without stabilizing particles.
2. A textured crystalline columnar structure was found on pure aluminium films, believed to result from directional solidification during film pulling.

3. AlSi9.5/SiC composite containing 20 vol.% SiC of 10 μm size gives a stable thick film. Reduction in SiC particle concentration leads to thinner films. This could be attributed mostly to a decrease in melt viscosity, which increases the liquid drainage out of the film prior to solidification.
4. AlSi9.5/SiC composite containing 5 vol.% SiC cannot produce stable films due to lack of sufficient numbers of particles.
5. The SiC particles between the film surfaces are well distributed, and this plays a key role in stabilizing the film. The degree of surface segregation has not yet been studied in detail.
6. Although TiB_2 particle are known to have poor wetting with Al, stable, smooth and thin films could be make from Al-6 vol.% TiB_2 composites made by in-situ reaction synthesis. Reduction in the particle concentration to 3, 1.5 and 0.6 vol.% resulted in stable and uniform thin films. Along with the melt viscosity, a decrease in TiB_2 cluster size is believed to be responsible for this change.
7. Al-0.6 vol.% TiB_2 particles can give stable, thin, and smooth films. The reduction in thickness obtained in the case of Al-0.6 vol.% TiB_2, in comparison to Al-3 vol.% TiB_2 films, is highly significant.
8. In-situ observation of film thickness and drainage in single liquid metal films was revealed that film thickness changes in time, showing decreases at the bottom and in the middle of the film (5.1±0.4 to 8.4±2.0 %), but increases at the top (5.3±1.5 %).

Acknowledgements:

Texture measurements by Michael Huppmann, TU-Berlin are gratefully acknowledged.

References

[1] M. F. Ashby, A. Evans, N.A. Fleck, L.J. Gibson, J.W. Hutchinson, H.N.G. Wadley, *Metal foams – a design guide*, Butterworth-Heinemann, Boston (2000).

[2] J. Banhart, *Manufacture, characterization and application of cellular metal foams*, Prog. Mater. Sci. (2001) 46:559–632.

[3] V. Gergely, T.W. Clyne, *Drainage in the standing liquid metal foams: modelling and experimental observation*, Acta Mater. (2004) 52:3047–3058.

[4] D.T. Wasan, A.D. Nikolov, L.A. Lobo, K. Koczo and D.A. Edwards, *Foams, thin films and surface rheological properties*, Prog. Surf. Sci. (1992) 39:119–154.

[5] J.H. Aubert, A.M. Kraynik and P.B. Rand, *Aqueous foams*, Scientific American (1986) 254:58–66.

[6] S.W. Ip, Y. Wang and J.M. Toguri, *Aluminium foam stabilisation by solid particles*, Can. Met. Quart. (1999) 38:81–92.

[7] D. Wang, Z. Shi, *Effect of ceramic particles on cell size and wall thickness of aluminium foam*, Mat. Sci. Eng. (2003) A361:45–49.

[8] J. Banhart, *Metal Foams: Production and Stability*, Adv. Eng. Mater., 8:781–794.

[9] G. Verbist, D. Weaire, A.M. Kraynik, *The foam drainage equation*. J. Phys: Condens. Matter (1996) 8:3715–3731.

[10] S.A. Koehler, S. Hilgenfeldt, H.A. Stone, *A generalized view of foam drainage: Experiment and theory*. Langmuir (2000) 16:6327–6341.

[11] A. Bhakta, E. Ruckenstein, *Foams and concentrated emulsions: dynamics and phase behavior*. Langmuir (1995) 11: 4642–4652.

[12] S.J. Neethling, J.J. Cilliers, E.T. Woodburn, *Prediction of the water distribution in a flowing foam*. Chem. Eng. Sci. (2000) 4021–4028.

[13] V. Carrier, S. Hutzler, D. Weaire, *Drainage of foam with regularly spaced parallel soap films*, Colloids and Surfaces A: Physiochem. Eng. Aspects (in press).

[14] R.J. Pugh, Foaming, *Foam films, antifoaming and defoaming*, Adv. Coll. Interface Sci. (1996) 64:67–142.

[15] B. Kriszt, P. Cekan, K. Faure, *Foamability of the Al-Si system*, In: Cellular Metals and Metal Foaming Technology (Ed.: J. Banhart, M.F. Ashby, N.A. Fleck), Verlag MIT, Bremen (2001) 77–82.

[16] H. Stanzick, M. Wichmann, J. Weise, L. Helfen, T. Baumbach, J. Banhart, *Process control in aluminum foam production using real-time x-ray radioscopy*, Adv. Eng. Mater. (2002) 4:814–823.

[17] C. Körner, F. Berger, M. Arnold, C. Stadelmann, R.F. Singer, *Influence of processing conditions on morphology of metal foams produced from metal powder*, Mat. Sci. Tech. (2000) 16:781–784.

[18] B. Olurin, M. Arnold, C. Körner, R.F. Singer, *The investigation of morphometric parameters of aluminum foams using micro-computed tomography*, Mat. Sci. Eng. (2002) A328:334-343.

[19] A.E. Markaki, T.W. Clyne, *Characterisation of impact response of metallic foam / ceramic laminates*, Mat. Sci. Tech. (2000) 16:785–791.

[20] G.S. Vinod Kumar, N. Babcsan, B.S. Murty, J. Banhart, *Verfahren zur Herstellung von Metallschäumen und Metalschaum*, (2007) German Patent Application DE 10 2006 031213.9.

[21] J.R. Davis, Aluminium and Aluminium Alloys, ASM International, Materials Park (1993).

[22] F. García-Moreno, M. Fromme, J. Banhart, *Real time X-ray radioscopy on metallic foams using a compact microfocus source*, Adv. Eng. Mater. (2004) 6:416–420.

[23] A. Haibel, A. Rack, J. Banhart, Why are metal foams stable? Appl. Phys. Lett. (2006) 89: 154102/1-3.

[24] N. Babcsán, J. Banhart, *Metal foams: towards high-temperature colloid chemistry*, In: Colloidal Particles at Liquid Interfaces (Eds: BP. Binks and T.S. Horozov), Cambridge University Press, Cambridge (2006), 445–499.

[25] N. Babcsan, D. Leitlmeier, H.P. Degischer, J. Banhart, *The role of oxidation in blowing particle-stabilised aluminium foams*, Adv. Eng. Mater. (2004) 6:421–428.

[26] N. Babcsan, D. Leitlmeier, J. Banhart, *Metal Foams - high temperature colloids. Part I. Ex-situ analysis of metal foams*, Coll. Surf. A: Physicochem. Eng. Asp. (2005) 261:123–130.

[27] N. Babcsan, G.S. Vinod Kumar, B. S. Murty, J. Banhart, *Grain refiners as liquid metal foam stabilizers*, Trans. Indian Inst. Met. (2007) 60:127–132.

[28] A. R. Kennedy, S. Asavavisitchai, *Effects of TiB_2 particles addition on the expansion, structure and mechanical properties of PM Al foams*, Scripta Mater. (2004) 50:115–119.

Table 1 Summary of different film pulling experiments.

alloy	particles (type, vol.%)	temp. (°C)	stable film?	thickness (μm)
Al	None	700	Yes	4 – 12
AlSi9.5	None	650,700	No	-
AlSi9.5	SiC, 20	650	Yes	21 – 45
AlSi9.5	SiC, 15	650	Yes	13 – 24
AlSi9.5	SiC, 10	650	Yes	10 – 23
AlSi9.5	SiC, 5	650	No	-
Al	TiB_2, 6	675	Yes	(> 30)*
Al	TiB_2, 3	675	Yes	> 37
Al	TiB_2, 1.5	675	Yes	> 24
Al	TiB_2, 0.6	675	Yes	> 16

** but with large variations*

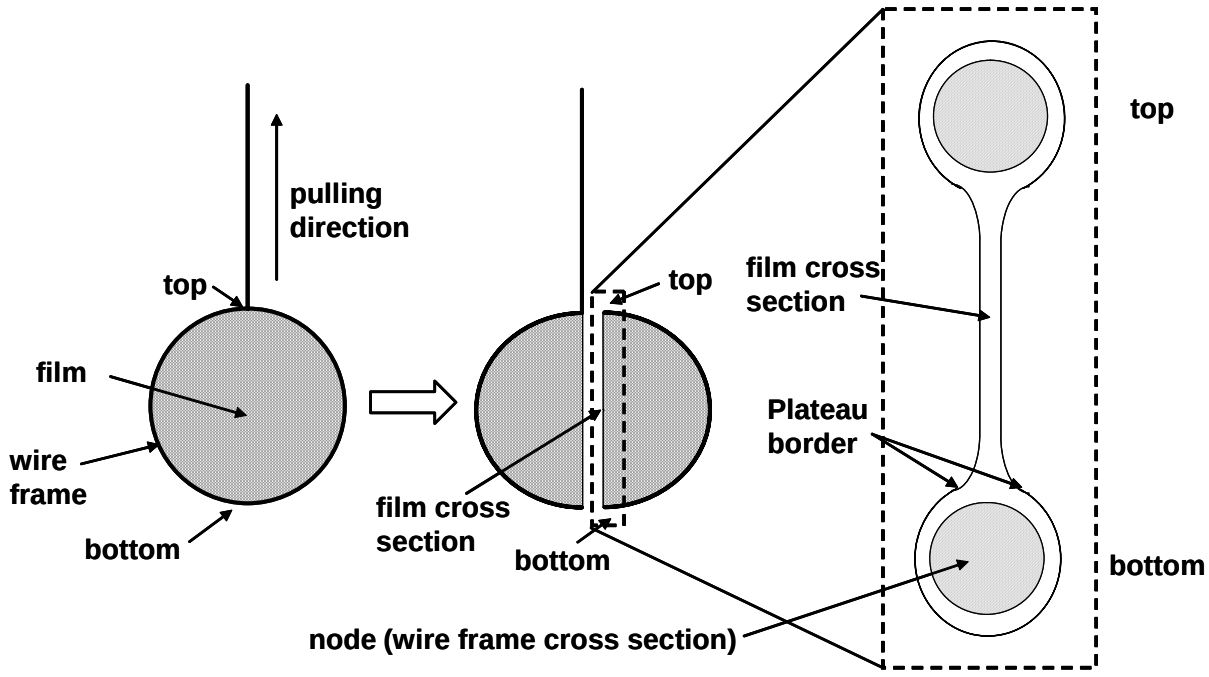

Fig. 1 Schematic of a metallic film cross section.

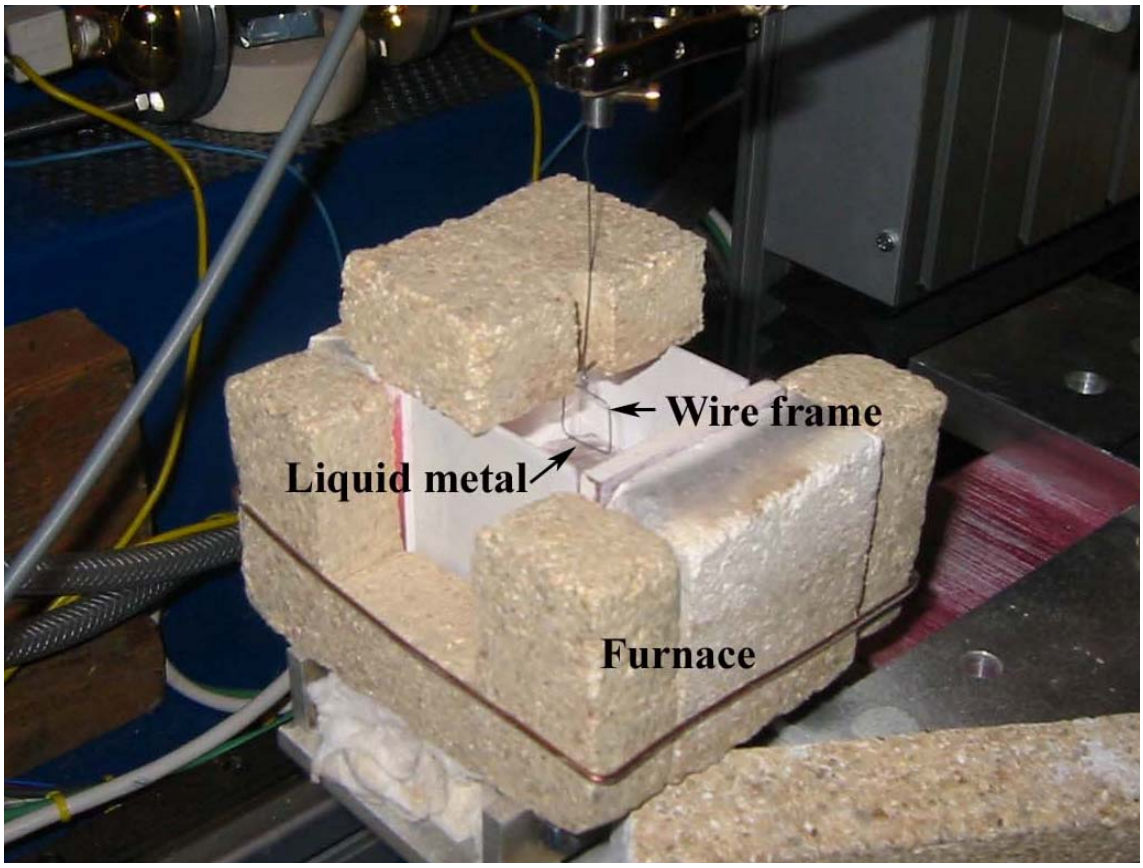

Fig. 2 Automatic film pulling setup and furnace inside the in-situ X-ray radioscopy unit.

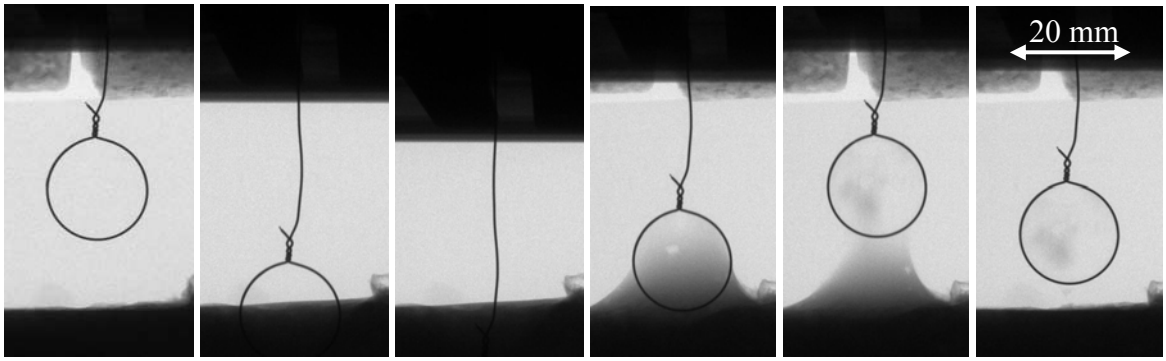

Fig. 3 Sequence of radioscopic images from a film pulling experiment using a circular Mo-wire (thickness = 0.5 mm, ring diameter = 20 mm) frame and an AlSi9/SiC/20p melt, T = 680 °C, v = 2.5 mm/s, a) t = 0 s, b) t = 11s, c) t = 20s, d) t = 48s, e) t = 55 s and f) t = 62 s.

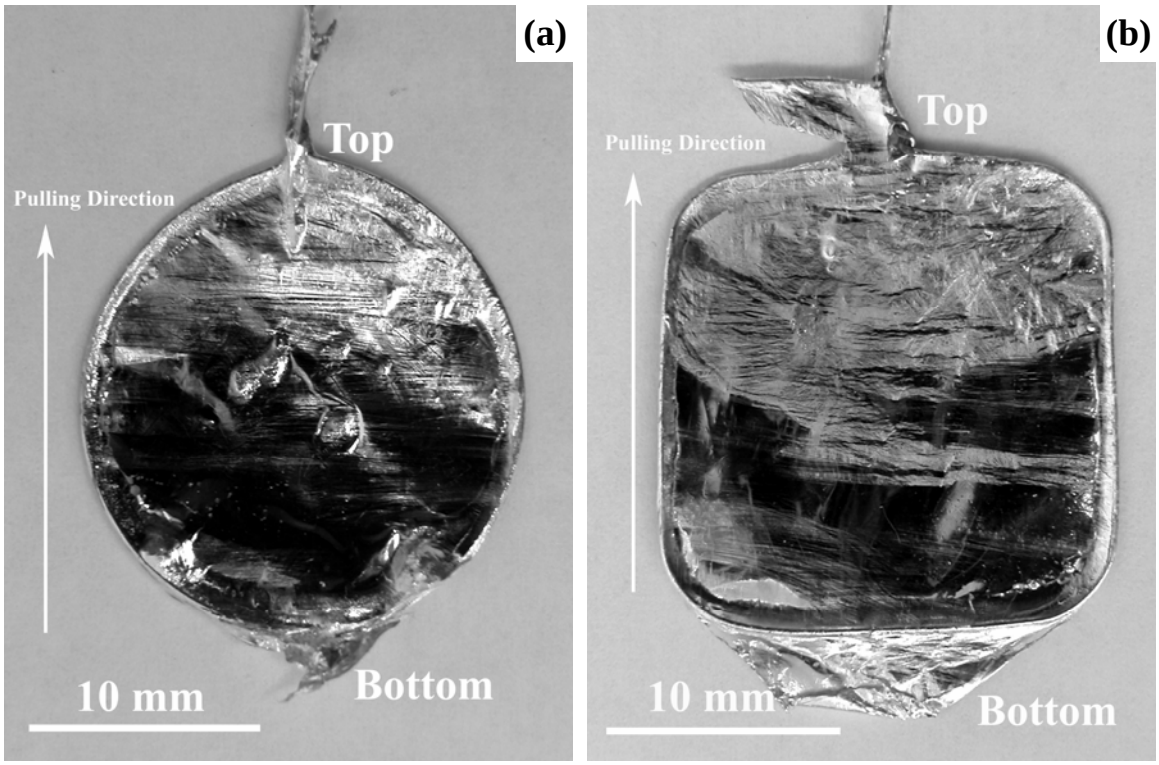

Fig. 4 Images of metallic films pulled from pure Al with (a) a circular wire frame and (b) a square wire frame, both made of stainless steel wire 0.4 mm thick.

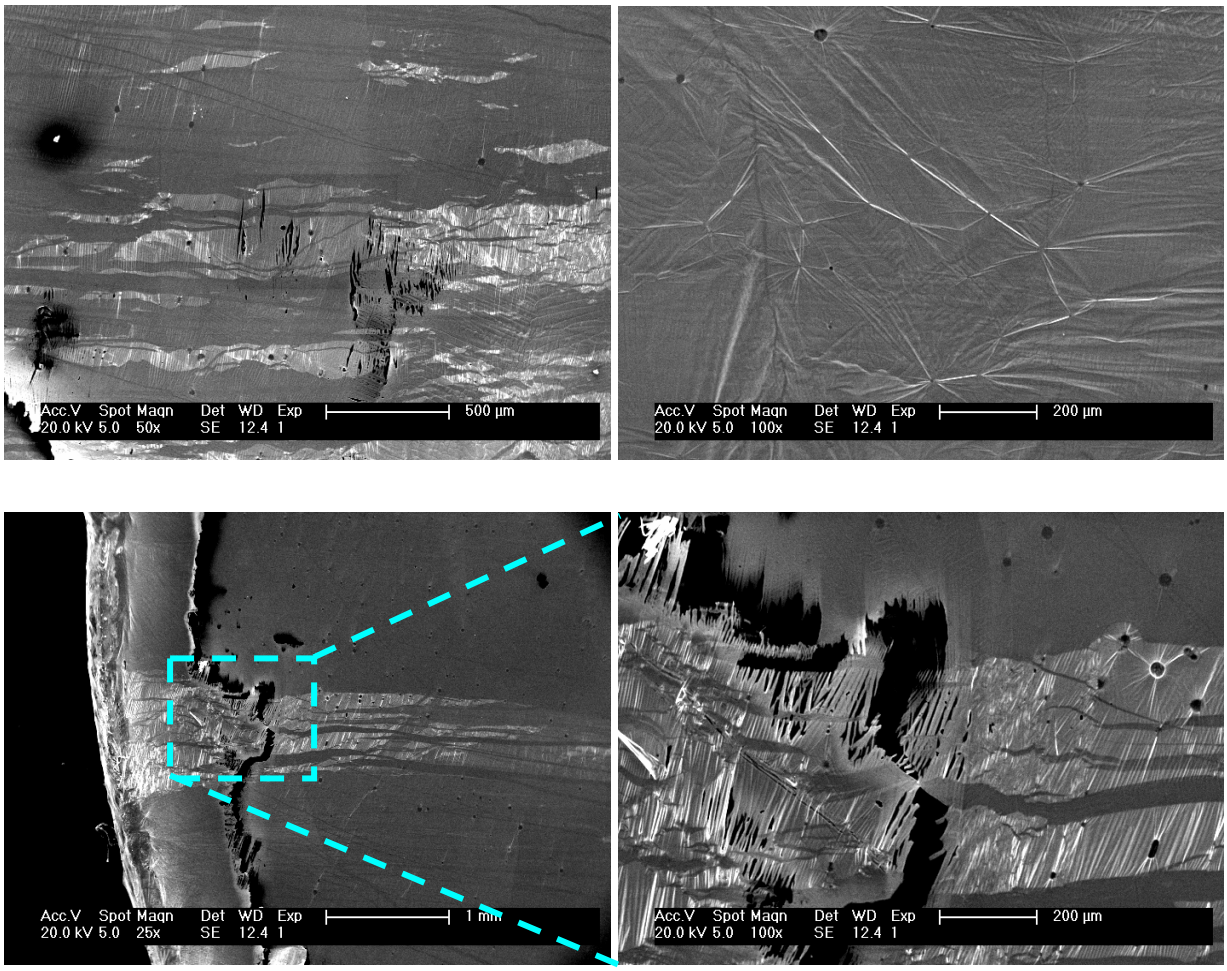

Fig. 5 SEM image of pure Al film surface. Cracks in the oxide skin perpendicular to the pulling direction and Al columns perpendicular to it can be observed.

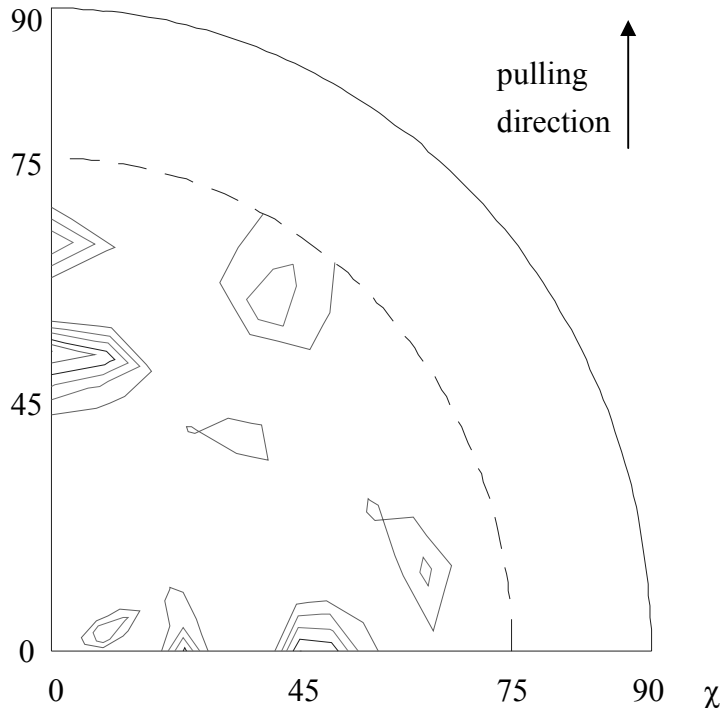

Fig. 6 Quarter of a (111) pole figure from a solidified aluminium film, corresponding to Fig. 5. A preferential orientation of the cubic structure can be observed, e.g. peaks at $\chi \sim 50°$.

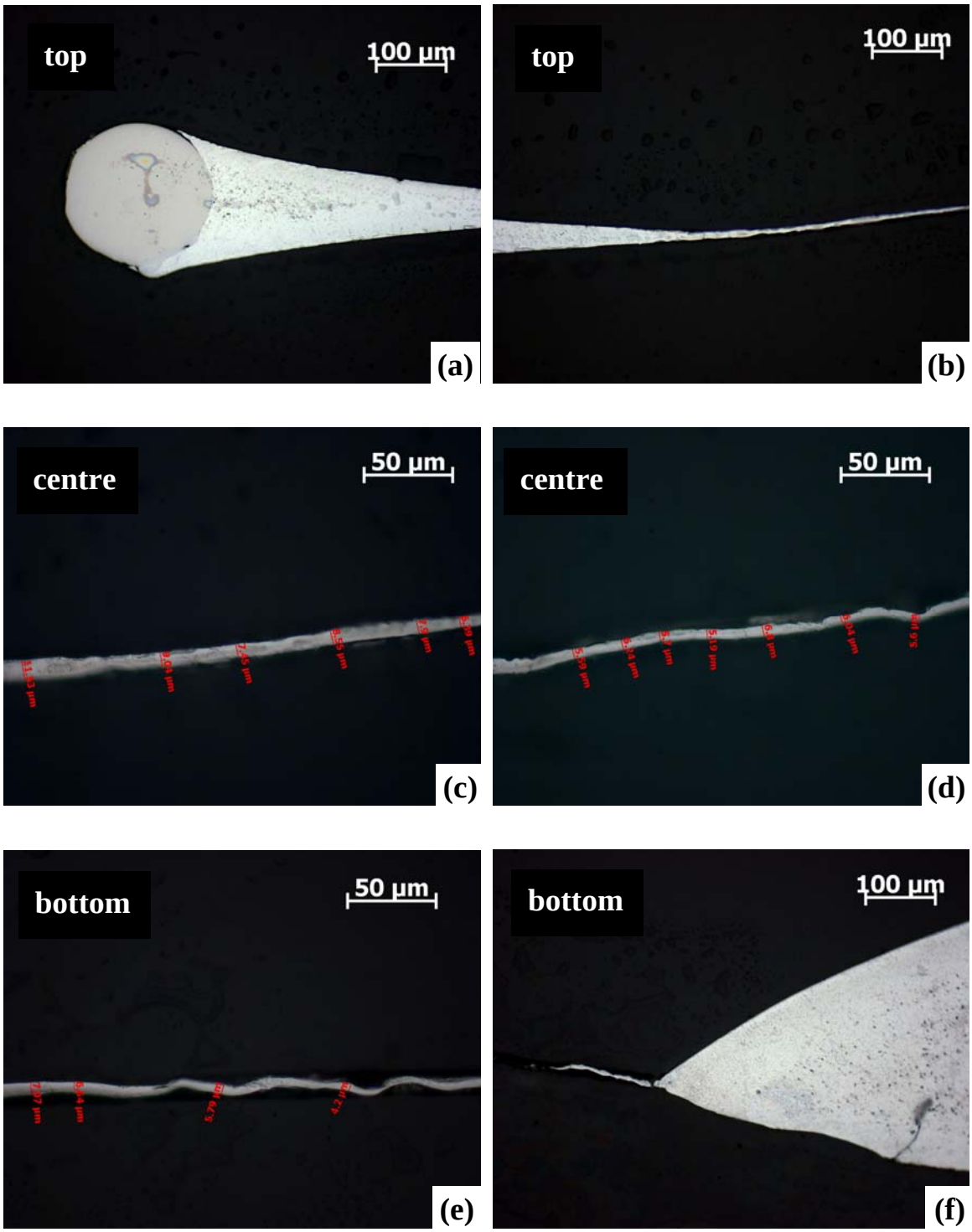

Fig. 7 Optical micrograph of a pure Al film cross section. (a) Top part of the film, showing node and Plateau border curvature, (b) subsequent thinning of the film, (c-d) centre part of the film, and (f) bottom part of the film showing cracking and drainage of the film.

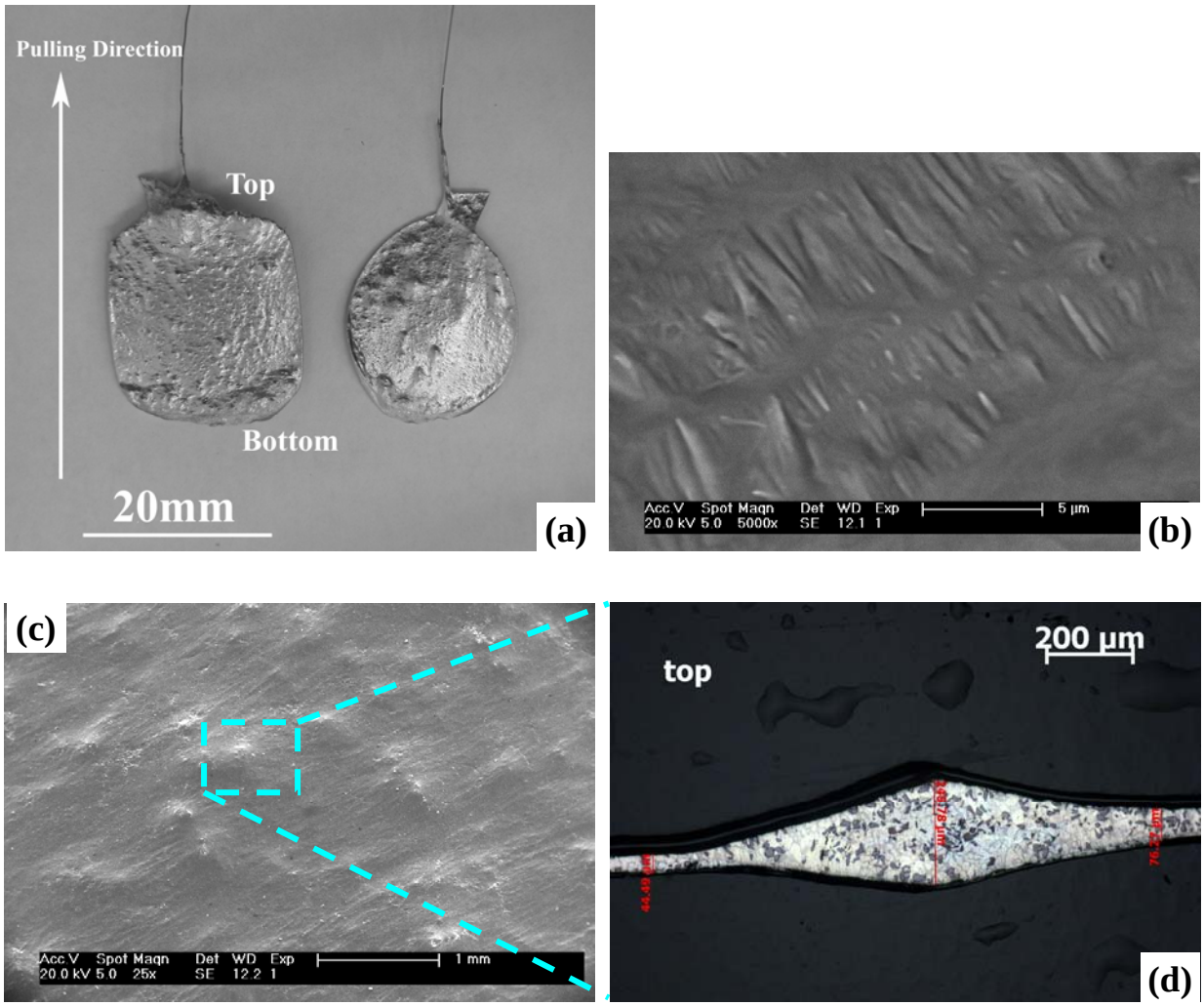

Fig. 8 (a) Photograph of AlSi9/SiC/20p composite films made using circular and square wire frames and SEM micrographs of (b) wrinkles in film surface, and (c) raises in film surface, (d) optical micrograph of the cross section of one elevations.

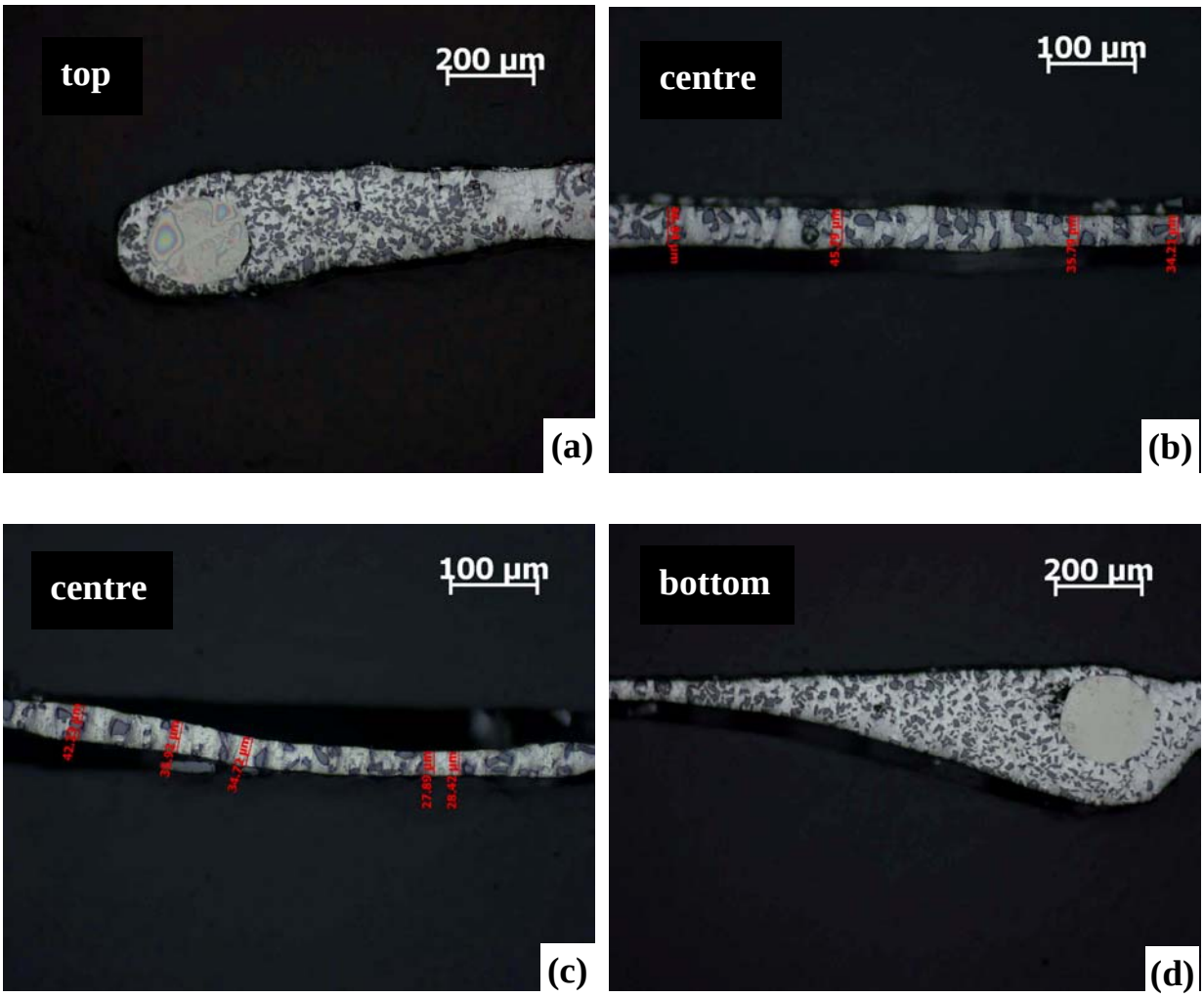

Fig. 9 Optical micrograph of the cross section of AlSi9/SiC/20p composite film (ring diameter 20 mm, stainless steel wire, 0.2 mm thick) (a) top part of the film shows node and Plateau border curvature, (b) and (c) centre part of the film (d) bottom part of the film.

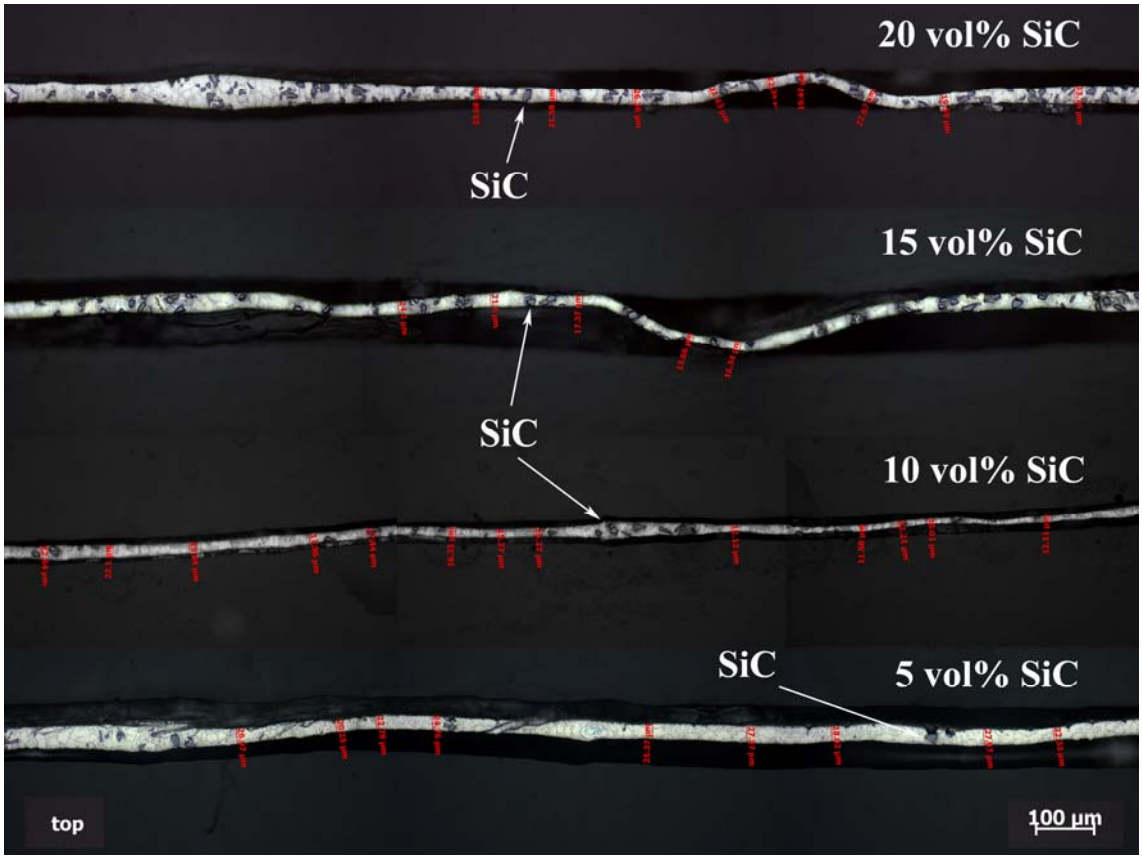

Fig. 10 Optical micrograph of the cross-section of AlSi9/SiC composite film at different volume contents of SiC particles. Ring diameter 20 mm, stainless steel wire, 0.2 mm thick. The first three images are equilibrium films, whereas the film with 5 vol.% SiC is an undamaged partial film obtained by fast withdrawal/pulling of the film.

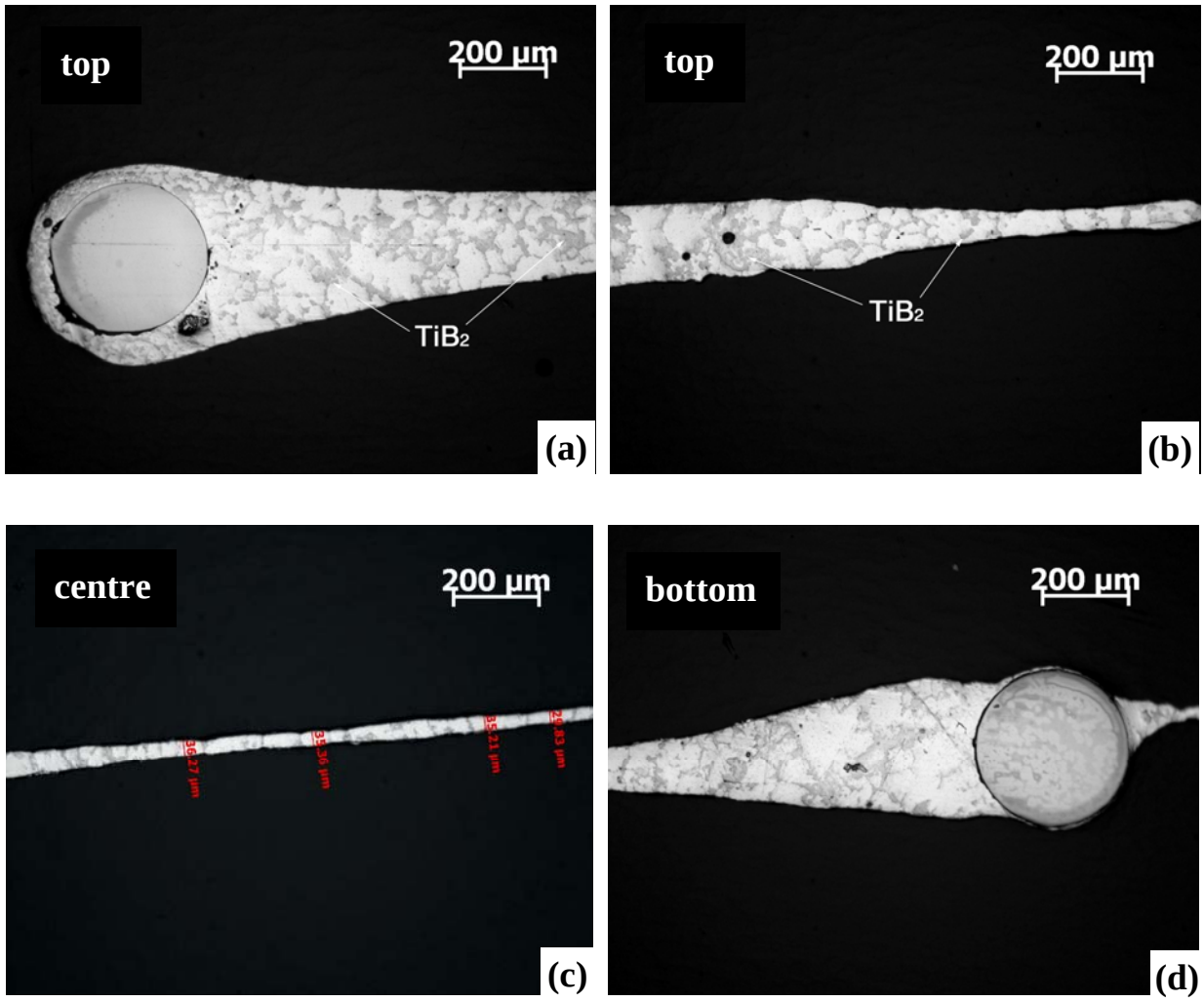

Fig. 11 Optical micrograph of the cross section of an Al/TiB_2/6p composite film (frame diameter 20 mm, stainless steel wire diameter 0.4mm). (a) and (b) top part of the film shows node and Plateau border curvature, (c) centre part of the film (d) bottom part of the film.

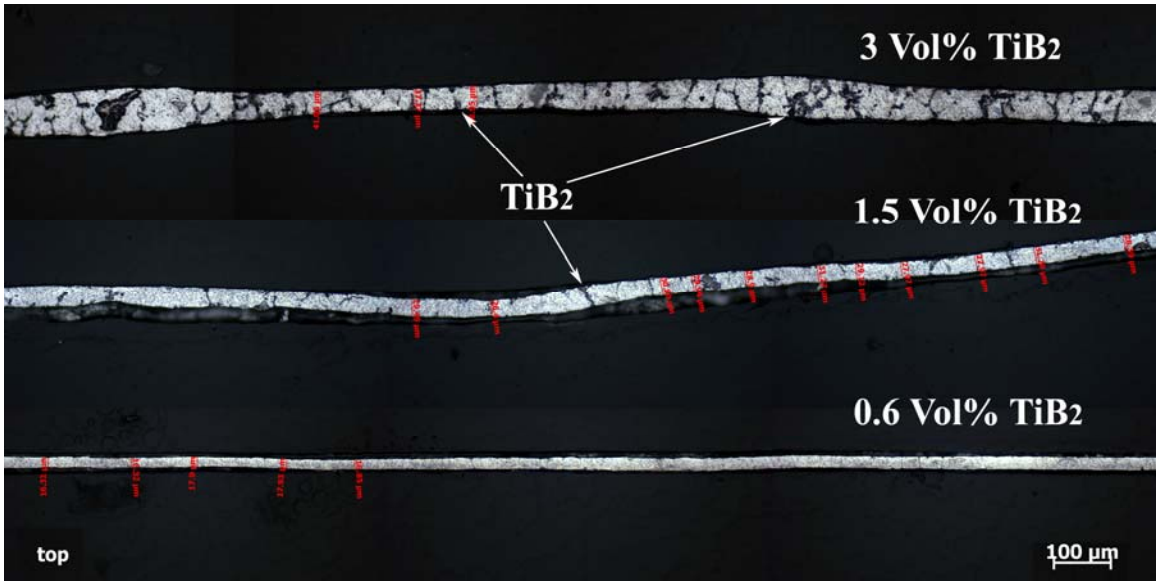

Fig. 12 Optical micrographs of the cross section of Al/TiB_2 films at different volume fractions of TiB_2 particles in an Al matrix.

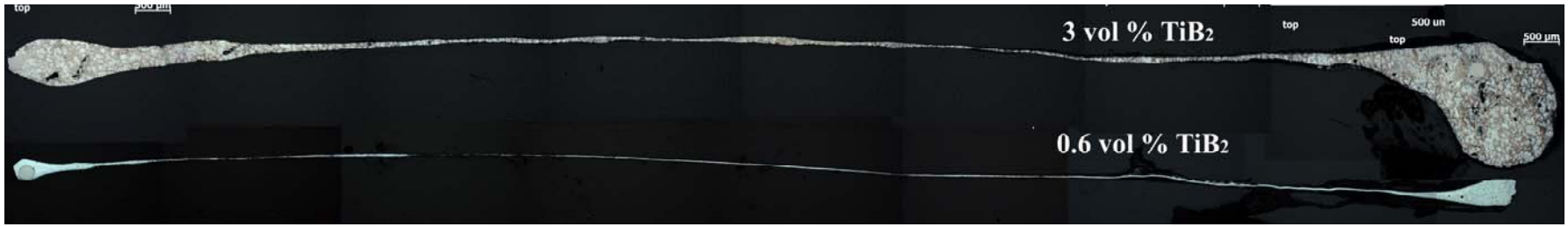

Fig. 13 Optical micrograph of the cross section of Al/ TiB_2/3p and Al/TiB_2/0.6p composite films.

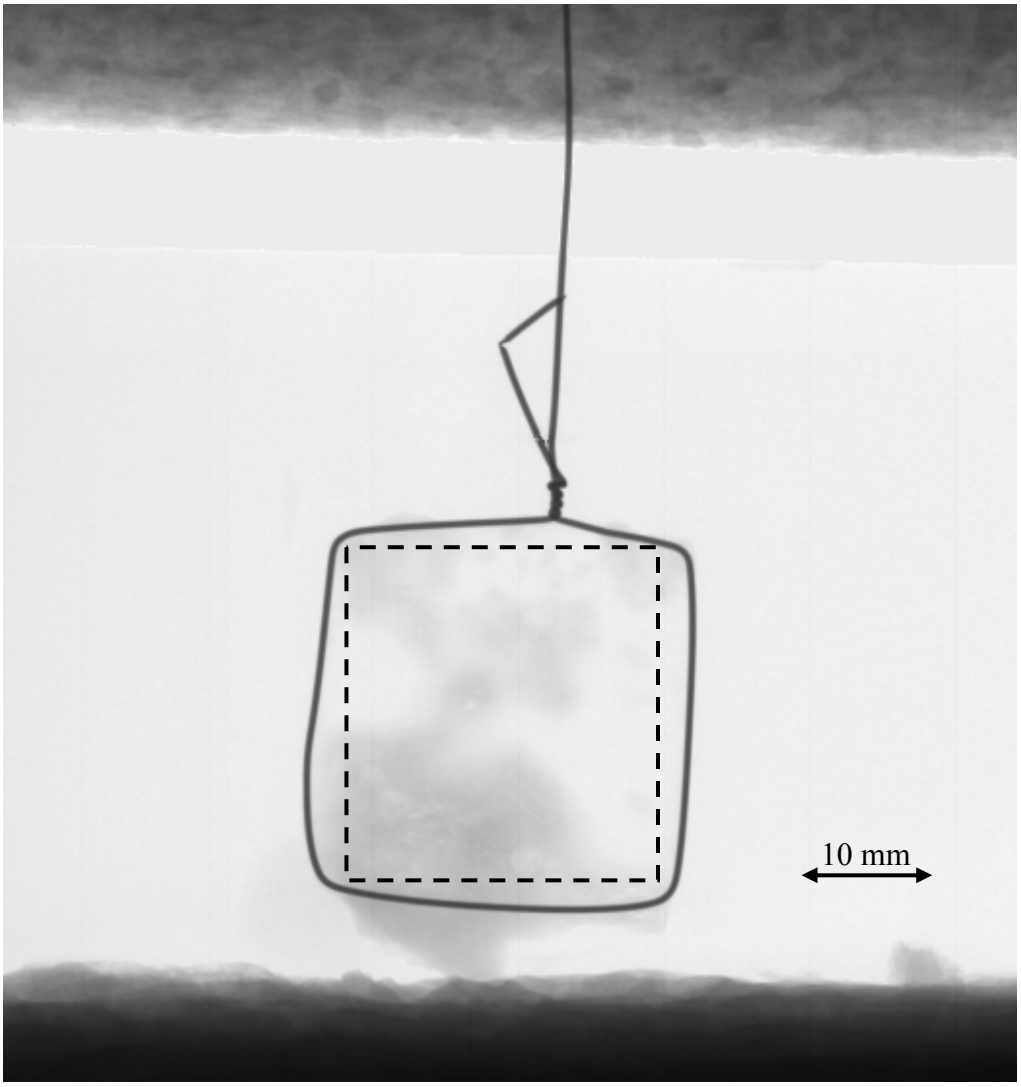

Fig. 14 Radioscopic images of a single film pulled from an AlSi9/SiC/5p melt using a square Mo-wire frame, T = 680°C; v = 2.5 mm/s. Dashed square marks the analysed region of interest.

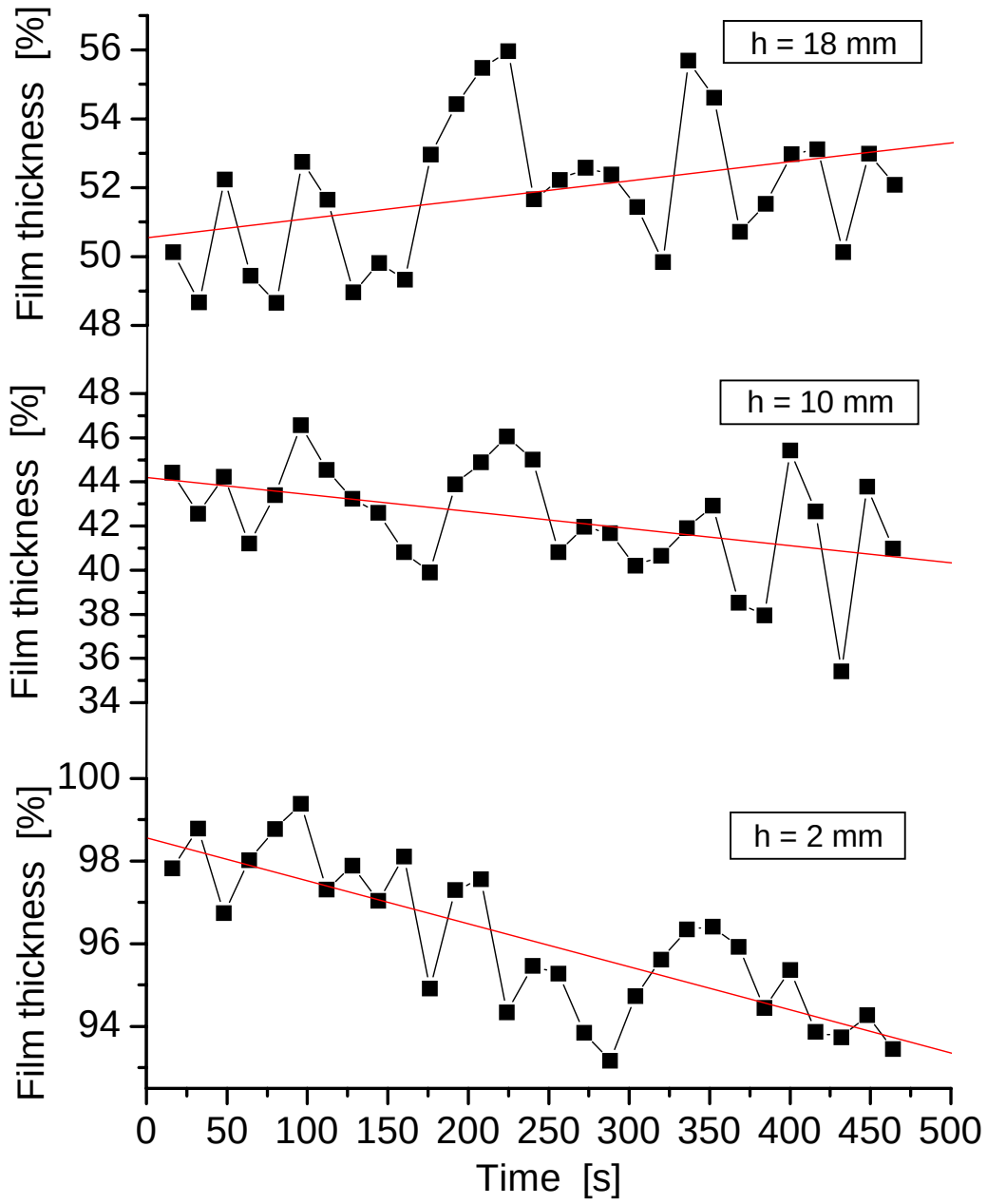

Fig. 15 Relative film thickness as defined in eq. (3) extracted from ROI in Fig. 14 at a height of (a) h = 2 mm, (b) h = 10 mm and (c) h = 18 mm from the bottom calculated from X-ray absorption images. For h = 2 and 10 mm the film thickness decreases by 5.1±0.4 and 8.4±2.0 % respectively. For h = 18 mm the film thickness increases by 5.3±1.5 %.